

Statistical Weight Kinetics Modeling and Estimation for Silica Nanowire Growth Catalyzed by Pd Thin Film

Qiang Huang, *Member, IEEE*, Li Wang, Tirthankar Dasgupta, Li Zhu, Praveen K. Sekhar, *Member, IEEE*, Shekhar Bhansali, *Member, IEEE*, and Yu An

Abstract—This work intends to understand and model the kinetic aspect or the change of substrate weight over time in the selective growth of silica nanowires (NWs) catalyzed through Pd thin film. Various adsorption-induced, diffusion-induced, or unified vapor-liquid-solid (VLS) growth models have been developed to describe the NW length varying with time. Since NW length has been difficult to be measured, substrate weight change is therefore used as an alternative in this study to investigate growth kinetics of NWs. We investigate six different weight kinetics models in predicting weight changes during growth. Model estimation and comparison are conducted using both maximum-likelihood estimation (MLE) and Bayesian approaches. Owing to the embedded kinetics information in the nonlinear growth models, the Bayesian hierarchical model is shown to be more desirable when process data is limited.

Note to Practitioners—Nanowires (NWs) have great potentials in electronic and photonic applications due to their unique properties. The repeatability of nanowire growth, however, is low and presents a major challenge for its mass production. Predictive modeling and control method is essential to the process yield and productivity improvement. The major difficulty of establishing such models is limited data and physical understanding of growth process. This paper provides a modeling approach to describe the overall NWs growth by modeling the weight changes over time in the growth of NWs.

Index Terms—Model selection, nanomanufacturing, nanostructure growth, process modeling.

I. INTRODUCTION

AMONG one-dimensional nanostructures, silica nanowires (NWs) have been investigated in recent years due to their photoluminescent properties and excellent biocompatibility.

Manuscript received January 07, 2010; revised May 26, 2010; accepted July 08, 2010. This paper was recommended for publication by Associate Editor M. K. Jeong and Editor K. Bohringer upon evaluation of the reviewers' comments. The work was supported in part by the National Science Foundation under Grant CMMI-0700659 and Grant CMMI-1002580.

Q. Huang and L. Wang are with the Daniel J. Epstein Department of Industrial and Systems Engineering, University of Southern California, Los Angeles, CA 90089 USA (e-mail: qiang.huang@usc.edu).

T. Dasgupta and L. Zhu are with the Department of Statistics, Harvard University, Cambridge, MA 02138 USA.

P. K. Sekhar is with the Materials Physics and Application Division, Los Alamos National Laboratory, Los Alamos, NM 87545 USA.

S. Bhansali is with the Department of Electrical Engineering, University of South Florida, Tampa, FL 33620 USA.

Y. An is with the Department of Industrial Management and Systems Engineering, University of South Florida, Tampa, FL 33620 USA.

Color versions of one or more of the figures in this paper are available online at <http://ieeexplore.ieee.org>.

Digital Object Identifier 10.1109/TASE.2010.2070493

Different approaches, such as laser ablation [1], oxide-assisted growth [2], sol-gel template method [3], carbothermal reduction [4], and gas-phase growth [5] (i.e., vapor-liquid-solid (VLS), solid-liquid-solid, vapor-solid growth) have been explored to synthesize these oxide NWs. The ability to produce stable NWs at desired locations in a controlled manner on planar substrates is of critical importance for fabricating NW-based devices such as nanoFETs, nanotransistors, and microphotonic nanosystems [6]. Sekhar *et al.* [7] reported selective growth of silica nanowires in silicon using Pt thin film as a catalyst. The mechanism of nanowire growth was established to follow the VLS model with the PtSi phase acting as the catalyst. The mechanism was validated by careful selection of Pt thickness, growth temperatures, and Ar gas flow. They claimed the advantages of the synthesis approach are: (a) tunable size and distribution of the parent nanoclusters; (b) its ability to form metal-dielectric hybrid configurations; and (c) a simple and cost effective solution for growing large-scale arrayable nanowires.

The objective of this research work is to understand, model, and estimate the kinetic aspect of the selective growth of silica NWs using Pd thin film, in particular, the change of substrate weight over time. Since the VLS mechanism was first introduced by Wagner and Ellis [8], both adsorption-induced VLS models [8]–[10] and diffusion-induced VLS models [10]–[12] have been developed. Ruth and Hirth [11] proposed a NW growth rate model: $dL/dt = 2\Omega/\tau(N_\infty - N_0)L/R$, if NW length $L \leq$ diffusion length $L_f = \sqrt{2D\tau}$, and $dL/dt = 2L_f\Omega(J - N_0/\tau)/R$, if $L > L_f$, where D is diffusion coefficient, τ is mean lifetime of the adatom on the NW sidewall, Ω is atomic volume of Si, J is impingement flux, R is NW radius, N_0 is adatom concentration at the liquid alloy, and N_∞ is adatom concentration at the base substrate. Dubrovskii *et al.* [10] developed a more complicated model to unify the two types of VLS models in molecular beam epitaxy. In either case, the length of NWs exhibits a rapid exponential growth at the beginning and a linear growth afterwards.

Extending the aforementioned kinetics models to our silica NW growth process in an open CVD furnace could be challenging, as it has completely different boundary conditions. NWs grown in open tube systems tend to curl and bundle which causes a metrology issue. Therefore, in this study we investigate the substrate weight change process or weight kinetics during VLS growth of silica NWs. We focus on identifying the proper weight kinetics model under uncertainties. The contribution is to obtain the engineering insight on weight changes during growth.

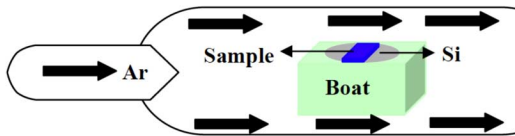


Fig. 1. Open tube furnace with Pd coated Si sample on support Si substrate.

II. EXPERIMENTAL DETAILS AND RESULTS

Prime grade 2" n-type silicon wafers were used as substrates for subsequent Pd deposition. Pd was sputtered onto Si substrate with film thickness being 5 nm. High purity Ar was chosen as carrier gas and was set to 25 SCCM throughout the course of the experiment. Prior to placing samples, the furnace was flushed with Ar for 10 min to minimize interference from gaseous impurities. Then, the sample was slowly introduced into the furnace along with a Si support wafer (Si Source), and heated up to 1100 °C. Once the furnace reached 1100 °C, the heating process was timed. Prior investigation [7] indicates the occurrence of melting process of Pd-Si during the ramp up to 1100 °C. Fig. 1 shows the experimental setup for NW growth.

A high-precision microbalance (Sartorius R200D) was used to measure the weight of the nanowire sample. The microbalance has a readout accuracy of 0.01 mg with a capacity to weigh up to 199.9999 g. The microbalance is typically calibrated with a known calibration standard before the sample measurement. After calibrating the equipment, the silicon sample is placed on a Whatman's filter paper, whose weight is zeroed-out before loading the sample. The sample is then covered by a plexiglass chamber to avoid any ambient noise causing spurious data. The sample is typically left for 10 seconds on the microbalance to get a stable reading and then the sample weight is recorded. The initial mass of the Pd coated Si sample was weighted and compared with the mass of the same sample after the NW growth for the desired time. A set of weight changes were recorded from 0.5 to 210 min with three replicates at each time point. Scanning Electron Microscopy (SEM, Hitachi S800) was used to image the sample surface after furnace treatment to observe the structure and morphology. The weight growth data is presented in Table I.

Fig. 2 shows the SEM micrograph of silica NWs observed at 15, 20, 60, and 90 min. It is evident that NWs are not straight with large variations among them. Hence, investigating overall weight changes make more sense to characterize this particular growth process. Fig. 3 illustrates the weight changes of Silica NWs during the growth period for three replicates. It is interesting to notice that the initial growth experienced weight loss. This might be due to source Si evaporation [13] and/or measurement error. In model fitting, we still retain the data before 15 min.

III. STATISTICAL WEIGHT KINETICS MODELING AND MAXIMUM-LIKELIHOOD ESTIMATION (MLE)

Let the random variable $y(t)$ denote the NW substrate weight change at time t , and let $E[y(t)] = \delta(t, \theta)$. In this section,

TABLE I
WEIGHT GROWTH DATA(mg)

Time(min)	Replicate 1	Replicate 2	Replicate 3
0.5	0.06	0.04	0.05
1	0.04	0.04	0.03
2	0.01	0.02	0.01
3	-0.02	-0.01	-0.01
4	-0.05	-0.06	-0.04
8	-0.24	-0.37	-0.27
10	-0.16	-0.2	-0.19
15	-0.15	-0.18	-0.14
20	0.01	0.013	0.012
30	2	1.33	1.352
45	2.56	2.42	2.45
60	5.16	6.26	5.95
75	8	7.66	7.82
90	8.84	9.42	9.21
100	9.72	9.67	9.59
120	9.91	9.96	9.97
150	10.1	10.3	10.3
180	10.4	10.4	10.3
210	10.5	10.3	10.4

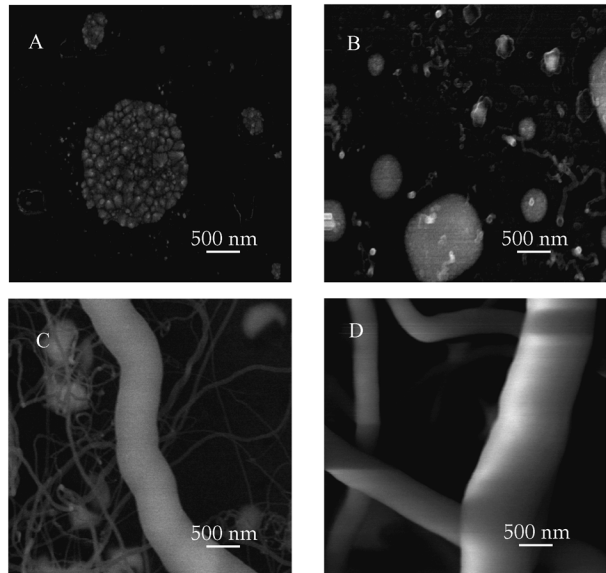


Fig. 2. SEM micrographs (25 KV, 20 K) illustrating the morphology of the Pd coated Si wafer heated at 1100 °C for (A) 15, (B) 20, (C) 60, and (D) 90 mins.

we shall consider different functional forms of $\delta(t, \theta)$ and examine how well they fit the data (t_i, y_i) , $i = 1, \dots, n$ obtained from our experiment. First, we shall consider a set of models for which the variance of $y(t)$ does not change with time. After identifying the most appropriate functional form $\delta(t, \theta)$ that explains the mean of the response, we will consider more generalized models with heteroscedasticity, that is, nonconstant variances.

A. Postulating and Fitting Models With Constant Error Variance

We now assume the following additive model with constant error variance:

$$y(t) = \delta(t, \theta) + \epsilon \quad (1)$$

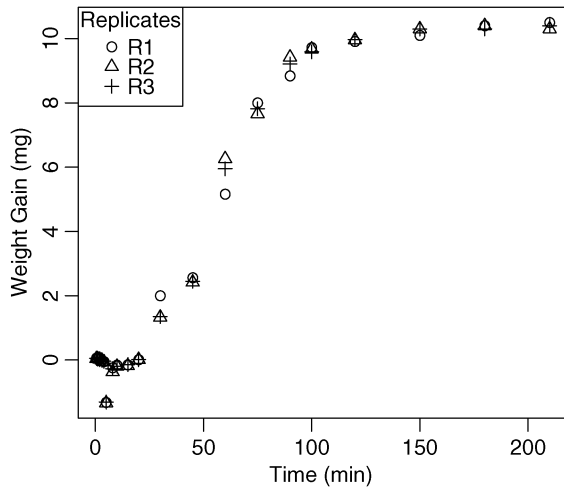


Fig. 3. Weight changes of silica NWs over time for three replicates.

where $\epsilon \sim N(0, \sigma^2)$, and postulate four possible functional forms for the mean term $\delta(t, \boldsymbol{\theta})$. The parameters of each model are estimated using by maximizing the likelihood function of the parameters (maximum-likelihood estimation or MLE). The variance of each estimate is obtained from the corresponding diagonal element of the inverse of the Fisher information matrix [14, Ch. 3], which is computed numerically.

Model 1. Exponential model: The curves of weight changes in Fig. 3 may simply suggest the following exponential model:

$$\delta(t, \boldsymbol{\theta}) = \alpha_1 \exp(-\alpha_2/t) \quad (2)$$

with parameters $\boldsymbol{\theta} = (\alpha_1, \alpha_2)$.

The log-likelihood function for this model is given by

$$L_1(\boldsymbol{\theta}, \sigma^2) = -\frac{1}{2\sigma^2} \sum_{i=1}^n (y_i - \alpha_1 \exp(-\alpha_2/t_i))^2 - \frac{n}{2} \log(\sigma^2). \quad (3)$$

The estimated parameters are: $\hat{\boldsymbol{\theta}} = (\hat{\alpha}_1, \hat{\alpha}_2) = (15.44, 59.85)$, $\hat{\sigma}^2 = 0.53$ with estimated standard deviations 0.49, 3.16, and 0.10, respectively. Akaike's information criterion, (popularly known as AIC and defined as $-2L + 2p$, where L is the maximized likelihood and p is the number of parameters), is computed as 132.03. It is evident from Fig. 4 that model 1 fails to capture the turning point of the growth curve and clearly deviates from the data at the late stage.

Model 2. Exponential-linear model with unknown change point t_0 and continuity at the first order derivative: Based on the weight change curves in Fig. 3 and previous growth rate models [10]–[12], [15], we can postulate the following exponential-linear model with unknown change point t_0 :

$$\delta(t, \boldsymbol{\theta}) = \begin{cases} \alpha_1 \exp(-\alpha_2/t), & t \leq t_0 \\ at + b, & t > t_0 \end{cases} \quad (4)$$

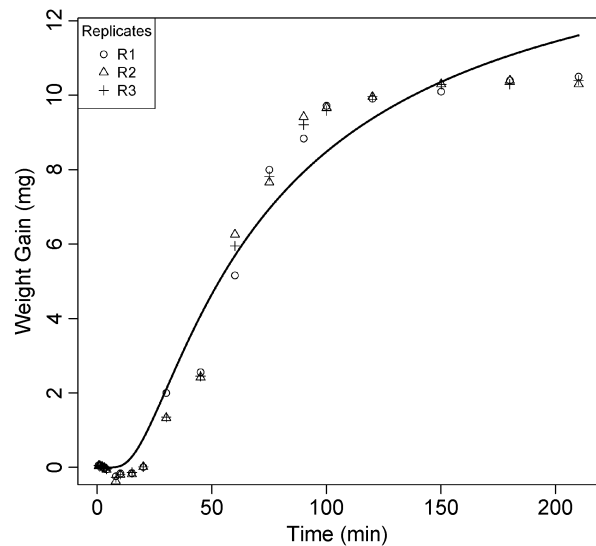


Fig. 4. Fitted curve of model 1.

with $\boldsymbol{\theta} = (\alpha_1, \alpha_2, t_0)$. Let $\delta_1(t) = \alpha_1 \exp(-\alpha_2/t)$, and $\delta_2(t) = at + b$. Assuming that the curve is continuous and differentiable at t_0 , it is easy to see that

$$a = \alpha_1 \left(1 - \frac{\alpha_2}{t_0}\right) e^{-\frac{\alpha_2}{t_0}}, \quad \text{and} \quad (5)$$

$$b = \frac{\alpha_1 \alpha_2}{t_0^2} e^{-\frac{\alpha_2}{t_0}} \quad (6)$$

so that model 2 is essentially a three-parameter model.

The log-likelihood function can be written as

$$L_2(\boldsymbol{\theta}, \sigma^2) = -\frac{n}{2} \log(\sigma^2) - \frac{1}{2\sigma^2} \sum_{i=1}^n \left[I_{t \leq t_0} (y_i - \alpha_1 \exp(\alpha_2/t_i))^2 + I_{t \geq t_0} (y_i - at_i - b)^2 \right] \quad (7)$$

where a and b satisfy (5), (6), and $I_A(t) = 1$, if $t \in A$, A can be any set; and 0, otherwise.

The estimates of $\hat{\alpha}_1$, $\hat{\alpha}_2$ and \hat{t}_0 are obtained as 15.43, 59.82, and 200, respectively. In this case, the parameter estimation degenerates to pure exponential estimation, which is undesirable.

Model 3. Exponential-linear model with unknown change point t_0 and continuity at t_0 : This model is the same as model 2, except for the fact that we do not impose continuity at the first order derivative, which is deemed as a much stronger assumption. This is thus a four-parameter model with $\boldsymbol{\theta} = (\alpha_1, \alpha_2, t_0, a)$ and log-likelihood function as

$$L_3(\boldsymbol{\theta}, \sigma^2) = -\frac{n}{2} \log(\sigma^2) - \frac{1}{2\sigma^2} \sum_{i=1}^n \left[I_{t \leq t_0} (y_i - \alpha_1 \exp(\alpha_2/t_i))^2 + I_{t \geq t_0} (y_i - at_i - b)^2 \right] \quad (8)$$

where $b = \alpha_1 \exp(-\alpha_2/t_0) - at_0$.

The estimates of $\hat{\alpha}_1$, $\hat{\alpha}_2$, \hat{a} , and \hat{t}_0 are 32.11, 105.65, 0.0092, and 86.37, respectively. The error variance is estimated as $\hat{\sigma}^2 = 0.086$ and the AIC is computed as 31.62.

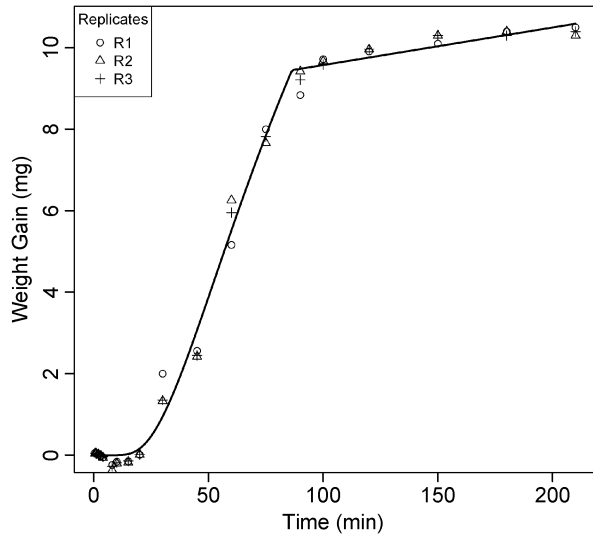


Fig. 5. Fitted curve of model 3.

The standard errors of $\hat{\alpha}_1$, $\hat{\alpha}_2$, \hat{a} , and \hat{t}_0 are estimated as 2.65, 5.29, 0.0016, and 2.16, respectively, while the standard error of $\hat{\sigma}^2$ is 0.016. We noticed from Fig. 5 that unlike models 1 and 2, the linear phase is captured and the resulting fit is much better than either of these models. Yet the transition between two phases seems not smooth.

Model 4. An exponential-linear model with a smooth transition function: In order to ensure a smooth transition between the linear and exponential phases without imposing the strong restriction of model 2 (that is, continuity at the first-order derivative or $\delta'_1(t_0) = \delta'_2(t_0)$), we introduce a transition function $h(t, \gamma)$ (see [16] and [17]) that joins the two phases

$$\delta(t) = [1 - h(t - t_0, \gamma)] \delta_1(t) + h(t - t_0, \gamma) \delta_2(t) + \epsilon \quad (9)$$

where $\boldsymbol{\theta} = (\alpha_1, \alpha_2, t_0, a, \gamma)$, $\epsilon \sim N(0, \sigma^2)$, and $h(t, \gamma)$ is continuous and smooth functions satisfying conditions listed in Appendix A.

Model 4 is a smooth approximation of $\delta(t)$, and the change point is included in a continuous and differentiable function $h(t - t_0, \gamma)$ so that it can be estimated together with other parameters. Based on $h(t, \gamma) = 1 - 1/(1 + \exp(t/\gamma^2))$ suggested in [17], we developed a transition function that satisfies a slightly different set of conditions (please refer to Fig. 6 and Appendix A), given the nature of $\delta_1(t)$ and $\delta_2(t)$ in model 4

$$h(t, \gamma) = \frac{\exp\left(\frac{t}{\gamma^2}\right) - \exp\left(\frac{-t_0}{\gamma^2}\right)}{1 + \exp\left(\frac{t}{\gamma^2}\right)}. \quad (10)$$

Comparing to the original transition function, our new transition function makes sure that when t approaching 0, the transition function's value is approaching 0 and thus makes sure that there is no transition function caused-bias around time 0.

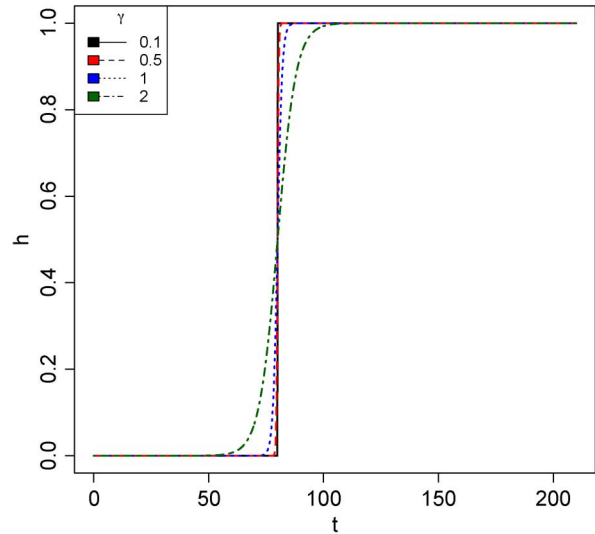
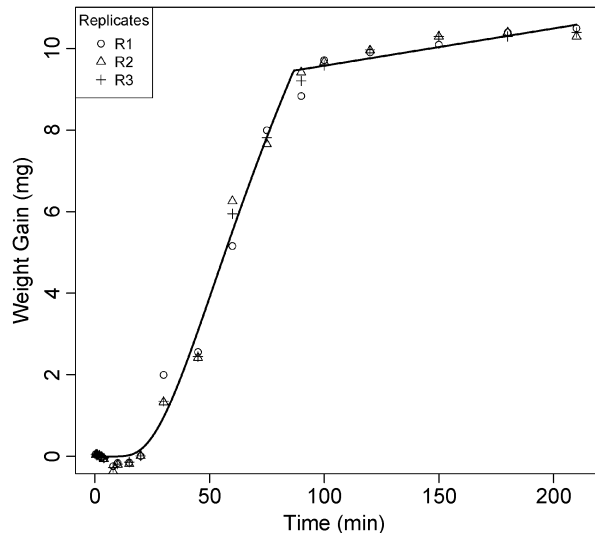

 Fig. 6. Transition function $h(t, \gamma)$ with different γ ($t_0 = 80$ s).


Fig. 7. Fitted curve of model 4.

The likelihood function is

$$L_4(\boldsymbol{\theta}, \sigma^2, \gamma) = -\frac{n}{2} \log(\sigma^2) - \frac{1}{2\sigma^2} \sum_{i=1}^n \{y_i - [1 - h(t_i - t_0, \gamma)] \times \delta_1(t_i) - h(t_i - t_0, \gamma) \delta_2(t_i)\}^2 \quad (11)$$

with $h(t, \gamma)$, $\delta_1(t)$, $\delta_2(t)$ defined above.

The estimates of $\hat{\alpha}_1$, $\hat{\alpha}_2$, \hat{a} , and \hat{t}_0 are 31.68, 104.85, 0.0091, and 86.77, respectively. The error variance $\hat{\sigma}^2$ is estimated as 0.086, and AIC is 31.71. The standard errors of $\hat{\alpha}_1$, $\hat{\alpha}_2$, \hat{a} , and \hat{t}_0 are estimated as 2.57, 5.18, 0.0016, and 2.20, respectively, while the standard error of $\hat{\sigma}^2$ is 0.016. The estimated $\hat{\gamma}$ is 0.604 with standard deviation 1.5, and this small $\hat{\gamma}$ assures that the distortion brought to the fitted curve by the transition function is very small. In fact, by checking Fig. 7, one can hardly see the smoothing effect and the fitted curve is very close to model 3's result. If we magnify the area around the transition point, as shown in the Fig. 8, one can see the transition is smooth.

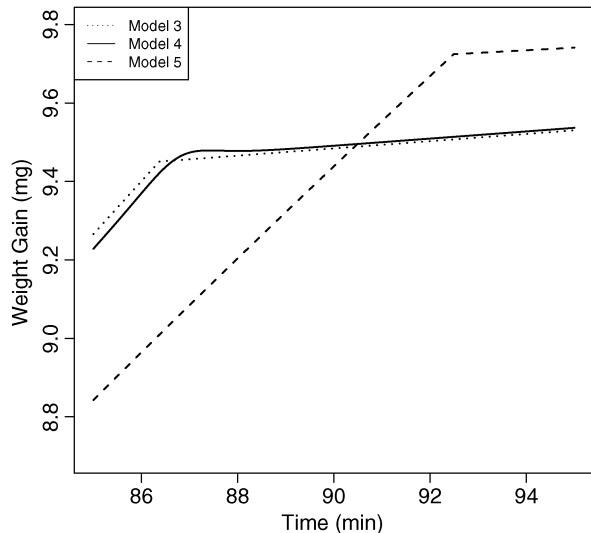


Fig. 8. Comparison of models 3, 4, and 5 near transition point.

 TABLE II
 PARAMETER ESTIMATION COMPARISON AMONG FOUR MODELS

		$\hat{\alpha}_1$	$\hat{\alpha}_2$	\hat{a}	\hat{t}_0	$\hat{\sigma}^2$
Model1	Avg	15.44	59.85	NA	NA	0.53
	Std	0.49	3.16	NA	NA	0.10
Model3	Avg	32.11	105.65	0.009	86.37	0.086
	Std	2.65	5.29	0.002	2.16	0.016
Model4	Avg	31.68	104.85	0.009	86.77	0.086
	Std	2.57	5.18	0.002	2.20	0.016
Model5	Avg	28.59	99.75	0.007	92.49	0.11,0.013
	Std	1.70	4.32	0.001	1.71	0.025,0.005

Model Comparison: The summary of MLE is given in Table II (note that Model 2 is degraded to Model 1). To compare models, we fit the first four models again using the first two replicates as training data and the third one as validation data. Clearly, models 1 and 2 are different (and much worse) as compared to models 3 and 4. The mean square errors (MSEs) are 0.537 for models 1 and 2, 0.0595 for model 3, and 0.0596 for model 4. Quite naturally, the question arises whether the gain obtained by introducing the complicated model 4 is substantial. To answer this question, we test the hypothesis $H_0 : \gamma = 0$ versus $H_1 : \gamma > 0$ using the likelihood ratio test (LRT). LRT statistics is constructed as $2 \times (L_4 - L_3)$, where L_3 and L_4 are the log-likelihood given by (8) and (11). (When $\gamma \rightarrow 0$, the transition model actually becomes model 3, i.e., the reduced model.) The likelihood ratio statistic asymptotically follows a χ^2 distribution with 1 df. The statistics is computed as 0.12 with a p -value of 0.725, which means there is not enough evidence to reject H_0 in favor of H_1 . Therefore, model 3 seems to be adequate to explain the mean part of the curve. Table II summarizes the MLE results for different models.

B. Generalizing to Heteroscedastic Model

Having identified model 3 as the best functional form for $\delta(t, \theta)$, we now try to make the model more realistic by considering the variance structure. The exponential phase in model 3 usually lasts shorter compared to the linear phase. It is relatively difficult to observe the growth during the initial period, making the inherent measurement error much larger during that

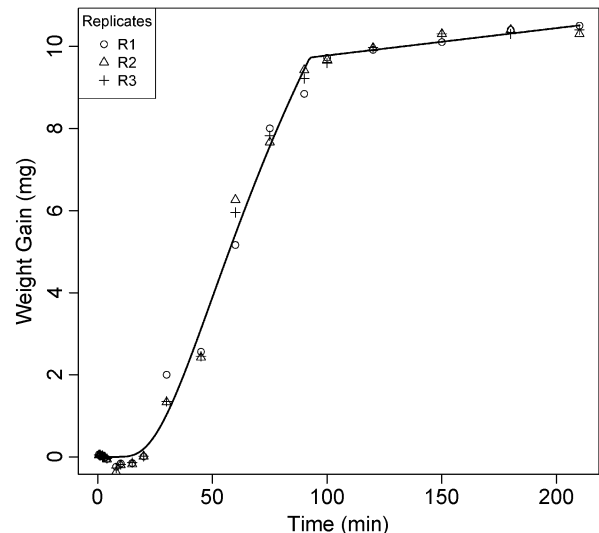


Fig. 9. Fitted curve of model 5.

period. To check whether the data reflects this, we consider the following modification of (1).

Model 5. *Exponential-linear with unequal variances in two phases:*

$$y(t) = \begin{cases} \delta_1(t, \theta) + \epsilon_1, & t \leq t_0 \\ \delta_2(t, \theta) + \epsilon_2, & t > t_0 \end{cases} \quad (12)$$

where $\delta_1(t)$ and $\delta_2(t)$, respectively, represent the exponential and the linear components of $E[y(t)]$ in model 3. As in model 3, we impose the continuity constraint $\delta_1(t_0, \theta) = \delta_2(t_0, \theta)$, so that we have $\theta = (\alpha_1, \alpha_2, t_0, a)$. We assume $\epsilon_1 \sim N(0, \sigma_1^2)$ and $\epsilon_2 \sim N(0, \sigma_2^2)$, where $\sigma_1^2 > \sigma_2^2$. The log-likelihood function for model 5 is

$$L_5(\theta, \sigma_1^2, \sigma_2^2) = \sum_{i=1}^N \left\{ I_{t \leq t_0} \left[-\frac{1}{2} \log(\sigma_1^2) - \frac{1}{2\sigma_1^2} (y_i - \alpha_1 \exp(\alpha_2/t_i))^2 \right] + I_{t > t_0} \left[-\frac{1}{2} \log(\sigma_2^2) - \frac{1}{2\sigma_2^2} (y_i - at_i - b)^2 \right] \right\}. \quad (13)$$

The estimated parameters are: $\hat{\theta} = (\hat{\alpha}_1, \hat{\alpha}_2, \hat{a}, \hat{t}_0) = (28.59, 99.75, 0.0067, 92.49)$, $\hat{\sigma}_1^2 = 0.11$, $\hat{\sigma}_2^2 = 0.013$ with standard errors $(\sigma_{\hat{\alpha}_1}, \sigma_{\hat{\alpha}_2}, \sigma_{\hat{a}}, \sigma_{\hat{t}_0}) = (1.70, 4.32, 0.00075, 1.71)$, $\sigma_{\hat{\sigma}_1^2} = 0.025$, $\sigma_{\hat{\sigma}_2^2} = 0.005$. The AIC is computed as 17.11. The fitted model is shown in Fig. 9. By comparing the estimated transition point from Fig. 8, we can see model 5 has slightly different and more accurate estimation, which is critical to pinpoint the change point of growth process.

To test our assumption of unequal variances, we conduct LRT of the hypothesis $H_0 : \sigma_1 = \sigma_2$ versus $H_1 : \sigma_1 > \sigma_2$. The LRT statistic is obtained as $2 \times (L_5 - L_3) = 9.86$, which is very significant with respect to a χ^2 distribution with 1 df. Therefore, it is reasonable to consider a model with unequal variances during the two phases.

IV. A BAYESIAN HIERARCHICAL MODEL FOR ESTIMATION WITH LIMITED OBSERVATIONS

In the previous section, we identified model 5 as the most appropriate model that accounts for the heteroscedasticity.

TABLE III
POSTERIOR INFERENCE OF MODEL 6

variable	mean	std	2.5%	97.5%	\hat{R}
α_1	27.82	1.751	24.56	31.34	1.000067
α_2	97.75	4.514	89.08	106.8	1.00058
a	6.63E-3	9.67E-4	4.70E-3	8.52E-3	0.9999926
t_0	93.36	2.041	90.29	97.73	1.000031
σ_1	.353	.041	.283	.444	0.9999975
σ_2	.139	.0330	.0922	.219	0.999996

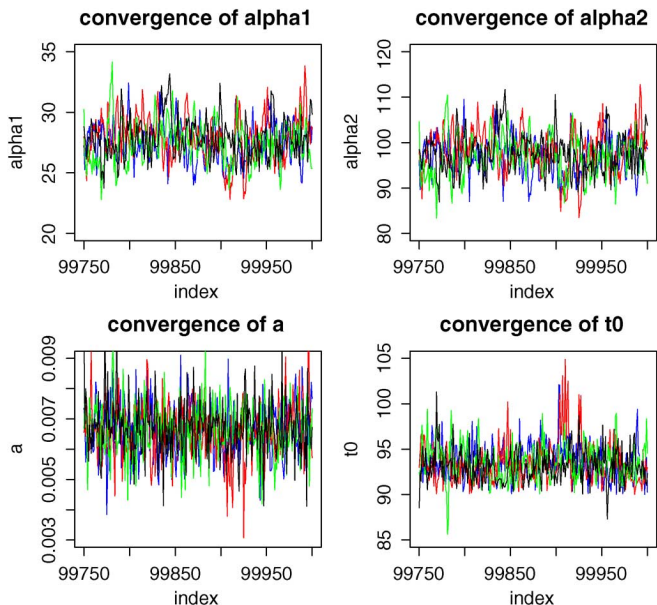


Fig. 10. Different chains simulated using WinBUGs.

Model 5 has a nice and realistic physical interpretation. However, the frequentist analysis suffers from the limitation that the standard errors of estimators are obtained by utilizing the asymptotic normality of the MLE. The accuracy of such an approximation will be questionable when limited observations are available (often the case in nanomanufacturing). The Bayesian hierarchical model considers the structure of multiple parameters and reflects the dependence among parameters in a joint probability model [18]. It not only incorporates all the features of model 5, but also utilizes available prior information about the parameters to address the concern of the lacking of data. We thus postulate the following model.

Model 6. A hierarchical exponential-linear model:

$$\begin{aligned}
 \text{Level 1: } & y \sim N(\mu, \sigma_\epsilon^2) \\
 \text{Level 2: } & \mu = I_{t \leq t_0} \alpha_1 \exp(-\alpha_2/t) \\
 & \quad + I_{t > t_0} (at + \alpha_1 \exp(-\alpha_2/t_0) - at_0) \\
 & \sigma_\epsilon^2 = I_{t \leq t_0} \sigma_1^2 + I_{t > t_0} \sigma_2^2 \\
 \text{Level 3: } & \text{Priors for } \theta = (\alpha_1, \alpha_2, t_0, a), \\
 & \text{and } \sigma_1^2, \sigma_2^2.
 \end{aligned} \tag{14}$$

The model at level 2 of the hierarchical framework is nothing but the model 5 discussed previously.

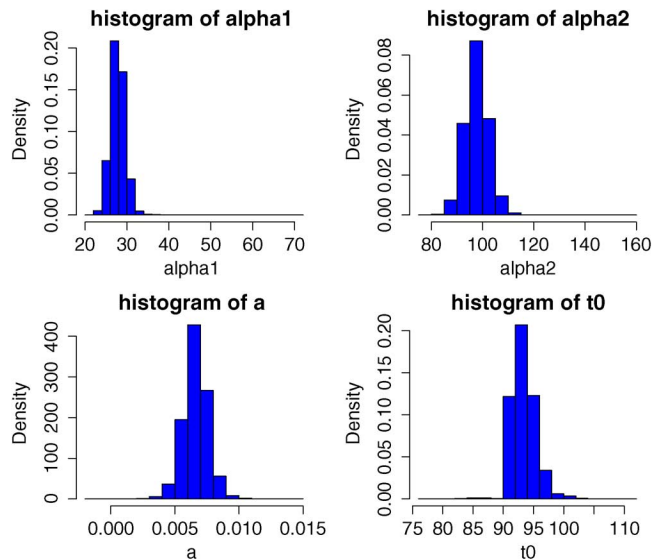


Fig. 11. Posterior distributions of α_1 , α_2 , a , and t_0 .

Assuming that we do not have any prior information before the experiment, we choose the following noninformative priors for estimation: $\sigma_1, \sigma_2 \sim Unif(0, 100)$, $t_0 \sim Unif(10, 150)$, $\alpha_1 \sim N(10, 10^4)$, $\alpha_2 \sim Unif(10, 300)$, and $a \sim N(0, 10^4)$.

Markov Chain Monte Carlo (MCMC) simulation [19] through WinBUGs software [20] was applied to draw from the posterior distributions of the parameters. We used four chains whose initial values were widely separated. The length of each chain is 100 000, but only the last 50 000 simulated values were used for inference while the first 50 000 observations were treated as draws during the “burn-in” period. A thinning rate of 100 was adopted to alleviate the auto-correlation. The convergence of different chains was confirmed by the Gelman–Rubin statistics \hat{R} which is close to 1. The simulation results are shown in Table III. Plots of different chains and histograms from the posterior draws of all the parameters shown in Figs. 10 and 11, respectively. Both these figures indicate convergence of the simulations.

V. CONCLUSION

In this study of the silica nanowire growth catalyzed by Pd thin film, we postulated six weight kinetics models based on the data collected under one growth condition. All the models were embedded with growth kinetics information. Through MLE and Bayesian hierarchical model estimation, we compared all the models. The exponential-linear model with unequal variances in two phases fits the data best.

Since the MLE utilizes the asymptotic normality, Bayesian hierarchical model is more suitable when data is limited. Particularly when we obtained confidence in the model structure from initial experimental study, Bayesian approach was shown to be more efficient for investigating new nanowire growth conditions. The future work will focus on investigating the effects of growth variables such as temperature on model parameters.

APPENDIX

PROOF FOR TRANSITION FUNCTION CHOICE

Given in [17], $h(t, \gamma)$ is continuous and smooth functions satisfying the following conditions:

$$\forall \gamma > 0 \lim_{t \rightarrow +\infty} (1 - h(t, \gamma)) \delta_1(t) = 0$$

$$\forall \gamma > 0 \lim_{t \rightarrow +\infty} (1 - h(t, \gamma)) \delta_2(t) = 0$$

$$\forall \gamma > 0 \lim_{t \rightarrow -\infty} h(t, \gamma) \delta_1(t) = 0$$

$$\forall \gamma > 0 \lim_{t \rightarrow -\infty} h(t, \gamma) \delta_2(t) = 0$$

$$\forall t \neq 0 \lim_{\gamma \rightarrow 0} h(t, \gamma) = \begin{cases} 1, & t > 0 \\ 0, & t < 0 \end{cases}$$

$$\forall \gamma > 0 h(t, \gamma), \quad h \text{ is non-decreasing in its domain.}$$

In our study, we noticed that as time can only be positive, we should make the third and fourth conditions stronger by changing $-\infty$ to 0.

In the following section, $\delta_1(t)$ and $\delta_2(t)$ are defined as in (4) and $h(t, \gamma)$ is defined in (10), then we can verify that:

$$\begin{aligned} & \forall \gamma > 0 \lim_{t \rightarrow +\infty} (1 - h(t, \gamma)) \delta_1(t) \\ &= \forall \gamma > 0 \lim_{t \rightarrow +\infty} \alpha_1 \exp\left(\frac{-\alpha_2}{t}\right) \frac{1 + \exp\left(\frac{-t_0}{\gamma^2}\right)}{1 + \exp\left(\frac{t}{\gamma^2}\right)} = 0 \\ & \forall \gamma > 0 \lim_{t \rightarrow +\infty} (1 - h(t, \gamma)) \delta_2(t) \\ &= \forall \gamma > 0 \lim_{t \rightarrow +\infty} \frac{(at + b) \left[1 + \exp\left(\frac{-t_0}{\gamma^2}\right)\right]}{1 + \exp\left(\frac{t}{\gamma^2}\right)} = 0 \\ & \forall \gamma > 0 \lim_{t \rightarrow 0} h(t, \gamma) \delta_1(t) \\ &= \forall \gamma > 0 \lim_{t \rightarrow 0} \alpha_1 \exp\left(\frac{-\alpha_2}{t}\right) \frac{\exp\left(\frac{t}{\gamma^2}\right) - \exp\left(\frac{-t_0}{\gamma^2}\right)}{1 + \exp\left(\frac{t}{\gamma^2}\right)} = 0 \\ & \forall \gamma > 0 \lim_{t \rightarrow 0} h(t, \gamma) \delta_2(t) \\ &= \forall \gamma > 0 \lim_{t \rightarrow 0} (at + b) \left[\frac{\exp\left(\frac{t}{\gamma^2}\right) - \exp\left(\frac{-t_0}{\gamma^2}\right)}{1 + \exp\left(\frac{t}{\gamma^2}\right)} \right] = 0 \\ & \forall t \neq 0 \lim_{\gamma \rightarrow 0} h(t, \gamma) \\ &= \begin{cases} \forall t \neq 0 \lim_{\gamma \rightarrow 0} \frac{\exp\left(\frac{t}{\gamma^2}\right) - \exp\left(\frac{-t_0}{\gamma^2}\right)}{1 + \exp\left(\frac{t}{\gamma^2}\right)} = 1, & t > 0 \\ \forall t \neq 0 \lim_{\gamma \rightarrow 0} \frac{\exp\left(\frac{t}{\gamma^2}\right) - \exp\left(\frac{-t_0}{\gamma^2}\right)}{1 + \exp\left(\frac{t}{\gamma^2}\right)} = 0, & t < 0 \end{cases} \\ h(t, \gamma) &= \frac{\exp\left(\frac{t}{\gamma^2}\right) - \exp\left(\frac{-t_0}{\gamma^2}\right)}{1 + \exp\left(\frac{t}{\gamma^2}\right)}, \end{aligned}$$

and it can be shown that partial derivatives are larger than 0 for all t and γ . All conditions are met with our choice of transition function.

REFERENCES

- [1] D. P. Yu, Q. L. Hang, Y. Ding, H. Z. Zhang, Z. G. Bai, J. J. Wang, Y. H. Zou, W. Qian, G. C. Xiong, and S. Q. Feng, "Amorphous silica nanowires: Intensive blue light emitters," *Appl. Phys. Lett.*, vol. 73, no. 21, pp. 3076–3078, 1998.
- [2] R. Zhang, Y. Lifshitz, and S. Lee, "Oxide-assisted growth of semiconducting nanowires," *ChemInform*, vol. 34, no. 24, 2003.
- [3] M. Zhang, E. Ciocan, Y. Bando, K. Wada, L. L. Cheng, and P. Pirouz, "Bright visible photoluminescence from silica nanotube flakes prepared by the sol-gel template method," *Appl. Phys. Lett.*, vol. 80, no. 3, pp. 491–493, 2002.
- [4] X. Wu, W. Song, K. Wang, T. Hu, B. Zhao, Y. Sun, and J. Du, "Preparation and photoluminescence properties of amorphous silica nanowires," *Chem. Phys. Lett.*, vol. 336, no. 1–2, pp. 53–56, 2001.
- [5] Z. Wang, "Nanobelts, nanowires, and nanodiskettes of semiconducting oxides—from materials to nanodevices," *Advanced Mater.*, vol. 15, no. 5, 2003.
- [6] L. Tong, J. Lou, R. R. Gattass, S. He, X. Chen, Lui, and E. Mazur, "Assembly of silica nanowires on silica aerogels for microphotonic devices," *Nano Lett.*, vol. 5, no. 2, pp. 259–262, 2005.
- [7] P. Sekhar, S. Sambandam, D. Sood, and S. Bhansali, "Selective growth of silica nanowires in silicon catalysed by pt thin film," *Nanotechnology*, vol. 17, no. 18, pp. 4606–4613, 2006.
- [8] R. S. Wagner and W. C. Ellis, "Vapor-liquid-solid mechanism of single crystal growth," *Appl. Phys. Lett.*, vol. 4, pp. 89–90, 1964.
- [9] E. Givargizov, "Fundamental aspects of VLS growth," *J. Crystal Growth*, vol. 31, pp. 20–30, 1975.
- [10] V. G. Dubrovskii, N. V. Sibirev, G. E. Girilin, J. C. Harmand, and V. M. Ustinov, "Theoretical analysis of the vapor-liquid-solid mechanism of nanowire growth during molecular beam epitaxy," *Phys. Rev. E*, vol. 73, p. 021603, 2006.
- [11] V. Ruth and J. P. Hirth, "Kinetics of diffusion-controlled whisker growth," *J. Chem. Phys.*, vol. 41, no. 10, pp. 3139–3149, 1964.
- [12] J. Kikkawa, Y. Ohno, and S. Takeda, "Growth rate of silicon nanowires," *Appl. Phys. Lett.*, vol. 4, p. 123109, 2005.
- [13] T.-H. Kim, "The structure and properties of silica thin films and nanowires," Doctoral dissertation, Australian National University, Canberra, 2010, unpublished.
- [14] J. Shao, *Mathematical Statistics (Texts in Statistics)*. New York: Springer, 2003.
- [15] Q. Huang, "Physics-driven Bayesian hierarchical modeling of nanowire growth process at each scale," *IIE Trans.*, 2010, (In press).
- [16] D. Bacon and D. Watts, "Estimating the transition between two intersecting straight lines," *Biometrika*, vol. 58, no. 3, p. 525, 1971.
- [17] R. Walkowiak and R. Kala, "Two-phase nonlinear regression with smooth transition," *Commun. Statistics-Simulation and Comput.*, vol. 29, no. 2, pp. 385–397, 2000.
- [18] D. Rubin, "Using empirical Bayes techniques in the law school validity studies," *J. Amer. Statist. Assoc.*, vol. 75, pp. 801–816, 1980.
- [19] J. S. Liu, *Monte Carlo Strategies in Scientific Computing*. New York: Springer, 2001.
- [20] D. Spiegelhalter, A. Thomas, N. Best, and D. Lunn, *WinBUGS User Manual*. [Online]. Available: <http://www.mrcbsu.cam.ac.uk/bugs>



Qiang Huang is currently an Assistant Professor at the Daniel J. Epstein Department of Industrial and Systems Engineering, University of Southern California, Los Angeles. He was an Assistant Professor and then an Associate Professor at the Department of Industrial and Management Systems Engineering, University of South Florida, from 2003 to 2009. Funded by the National Science Foundation, his research focuses on modeling and analysis of complex systems for quality and productivity improvement, with special interest in nanomanufacturing and

nanoinformatics.

Dr. Huang is a member of the Institute of Industrial Engineers (IIE), the Institute for Operations Research and the Management Sciences (INFORMS), SME, ASME, and MRS. He has served as an Associate Editor (Quality, Micro and Nanomanufacturing Systems) for the *SME Journal of Manufacturing Systems* since 2008. He is an editor for the Special Issue of the *IIE Transactions on Quality and Reliability Engineering/Manufacturing and Design*: "Quality, Sensing and Prognostics Issues in Nanomanufacturing." He is a member of the scientific committee (Editorial Board) for the North American Manufacturing Research Institution (NAMRI) of SME, 2009–2011. He has been an Associate Editor (Automation in Meso, Micro and Nano-Scale) for 2009 and 2010 IEEE Conference on Automation Science and Engineering.



Li Wang was born in Kunming, China. He received the B.S. degree in industrial engineering from Tsinghua University, Beijing, China, 2009. Since 2009, he is a graduate student at the University of Southern California, Los Angeles.

Mr. Wang is a member of the Institute for Operations Research and the Management Sciences (INFORMS).



Tirthankar Dasgupta received the Ph.D. degree in industrial engineering from the Georgia Institute of Technology, Atlanta.

He is currently an Assistant Professor of Statistics at Harvard University, Cambridge, MA. His research interests include design of experiments, statistical and engineering process control, application of statistics in nanotechnology, quality engineering, and quality management. He currently serves as an Associate Editor for *Technometrics*.

Dr. Dasgupta is a member of the American Statistical Association and the Institute for Operations Research and the Management Sciences (INFORMS).



Li Zhu was born on March 1985, in Nanjing, China. He received the B.S. degree in pure mathematics from Tsinghua University, Beijing, China, 2007. Currently, he is working towards the Ph.D. degree at the Department of Statistics, Harvard University, Cambridge, MA.

He is also a Research Assistant in Statistics at Harvard University under the supervision of Prof. Dasgupta. Previous to his Ph.D. experience at Harvard University, he had been a Research Assistant at the Center of Probability and Statistics, Tsinghua University, JiangSu Agriculture of Academy in China.

University, JiangSu Agriculture of Academy in China.



Praveen K. Sekhar (M'08) received the B.E. degree (with distinction) in electrical and electronics engineering from the Coimbatore Institute of Technology (CIT), Coimbatore, India, in 2001, and the M.S. degree in microelectronics and the Ph.D. degree in electrical engineering from the University of South Florida (USF), Tampa, in 2005 and 2008, respectively.

He is currently a Postdoctoral Research Associate in the Materials Physics and Applications Division (MPA-11), Los Alamos National Laboratory, Los Alamos, NM. His current research includes the areas of solid-state gas sensors, nanoengineered surfaces, microsystems and applied statistics.

Dr. Sekhar was the recipient of the Outstanding Dissertation Award from USF, Tampa.



Shekhar Bhansali (M'98) received the B.E. degree (Hons) in metallurgical engineering from the Malaviya Regional Engineering College (MREC), Jaipur, India, in 1987, the M.Tech. degree in aircraft production technology from the Indian Institute of Technology (IIT), Chennai, India, in 1991, and the Ph.D. degree in electrical engineering from the Royal Melbourne Institute of Technology (RMIT), Melbourne, Victoria, Australia in 1997.

He is currently a Professor at the Department of Electrical Engineering and the Nanomaterials and Nanomanufacturing Research Center, University of South Florida, Tampa. His current research includes the areas of biomicroelectromechanical systems (MEMS), sensors, nanomaterials and microsystems.

Dr. Bhansali was the recipient of a National Science Foundation (NSF) CAREER Award.



Yu An was born in TianJin, China, in 1983. He received the B.S. and M.S. degree in automation from TianJin University, TianJin, China, in 2006 and 2008, respectively.

He is currently a graduate student at the University of South Florida since 2008.